Chemical Science

ROYAL SOCIETY OF CHEMISTRY

EDGE ARTICLE

View Article Online
View Journal | View Issue

Cite this: *Chem. Sci.*, 2026, **17**, 8595

All publication charges for this article have been paid for by the Royal Society of Chemistry

Efficient near-infrared-excitable quantum dot-based triplet–triplet annihilation upconversion with a record anti-Stokes shift *via* low coverage of mono-styryl-BODIPY ligands

Ran Li,[a] Lin-Han Jiang,[a] Lin Xi,[b] Ming-Yu Zhang,[a] Hong-Juan Feng,[a] Dong-Xue Guo,[a] Lili Hou,[b] Ling Huang *[a] and Dai-Wen Pang *[a]

Ligands anchored on quantum dot surfaces with matched energy levels can significantly enhance triplet–triplet annihilation photon upconversion. In this study, we report a novel surface ligand (monosubstituted styryl-BODIPY) on near-infrared-absorbing lead sulfide quantum dots (PbS QDs) that achieves a high triplet exciton transfer efficiency of 65.4% as determined by femtosecond transient absorption spectroscopy, with an average of only seven ligands per quantum dot. Using rubrene as the annihilator, an upconversion efficiency of up to 16.8% ± 0.6% (normalized to 100%) is observed. Our newly developed BODIPY-derived ligand exhibits enhanced stability compared to widely reported tetracene-based surface ligands. Furthermore, its higher T_1 energy level allows coupling with the cyan-emitting annihilator 9,10-bis(phenylethynyl)anthracene, achieving a significant anti-Stokes shift from 808 nm excitation to 480 nm emission—an advancement not previously realized in NIR-excited QD-based TTA-UCs. This work provides a new opportunity, from the perspective of ligand design, to enhance quantum dot-based upconversion performance and expand the TTA-UC anti-Stokes shift using QDs into the cyan blue region, thereby advancing the development of efficient and stable upconversion materials.

Received 26th January 2026
Accepted 28th February 2026

DOI: 10.1039/d6sc00714g

rsc.li/chemical-science

Introduction

Near-infrared-excited triplet–triplet annihilation upconversion (NIR TTA-UC) holds broad application potential in solar energy utilization,[1–3] photocatalysis,[4–6] and biomedicine[7] by converting two low-energy photons into one higher-energy photon. Recently, quantum dot (QD)-based TTA-UCs have attracted broad interest. Unlike small-molecule-based TTA-UC, high-performance QD-based TTA-UC employs photosensitizers composed of QDs coupled with energy-level-matched surface ligands. The mechanism involves the QD absorbing low-energy photons and transferring energy to the surface ligand *via* triplet exciton transfer, populating the ligand's triplet state. This long-lived triplet ligand then sensitizes the annihilator in solution through triplet energy transfer (TET), promoting the annihilator to its triplet state. Finally, two triplet-excited annihilator molecules undergo triplet–triplet annihilation (TTA), where one molecule is upconverted to the singlet excited state and emits a higher-energy photon, while the other relaxes to the ground state.[8] Significant advances have been made in 808 nm-excited QD-based TTA-UC, with reports of high upconversion efficiencies. For instance, under 808 nm excitation, NIR TTA-UC using InAs,[9] $CuInSe_2$,[5] PbS,[10] and $AgBiS_2$ [11] QDs has achieved upconversion efficiencies (η_{UC}, normalized to 100%) of 21.1%, 16.7%, 13.5%, and 10.5%, respectively.

Although several NIR-excited QD-based TTA-UCs with relatively high efficiencies have been reported, a closer look at the development of this field reveals that current strategies for improving efficiency have mainly focused on controlling QD synthesis, composition, and morphology.[5,9,11,12] However, according to the mechanism of QD-based TTA-UC, surface ligands play a crucial role in enhancing upconversion performance.[13,14] Extensive research indicates that anchoring organic ligands with matched energy levels on the surface of NIR-excitable QDs can significantly enhance upconversion performance.[13,14] To date, carboxyl-substituted tetracene derivatives have been the primary surface ligands employed.[12,15,16] However, high η_{UC} values are typically observed only with high ligand surface coverage; for instance, InAs QDs require as many as 25 ligands per QD to achieve intense upconversion emission.[9] Unfortunately, an excessive number of large π-conjugated ligands often introduces surface defects and impairs the

[a]*Frontiers Science Center for New Organic Matter, Research Center for Analytical Sciences, Tianjin Key Laboratory of Biosensing and Molecular Recognition, State Key Laboratory of Medicinal Chemical Biology, Haihe Laboratory of Sustainable Chemical Transformations, College of Chemistry, Nankai University, Tianjin 300071, P. R. China. E-mail: huangl1@nankai.edu.cn; dwpang@whu.edu.cn*

[b]*State Key Laboratory of Precision Measurement Technology and Instruments, School of Precision Instruments and Optoelectronics Engineering, Tianjin University, 92 Weijin Road, Tianjin, 300072, China. E-mail: lilihou@tju.edu.cn*

dispersibility of QDs in solution.[17] Additionally, the tetracene derivatives typically possess triplet energies below 1.3 eV.[9] Such molecules exhibit poor stability and are readily degraded by trace amounts of reactive oxygen species,[17] which severely hinders the practical application of NIR-excited QD-based TTA-UC. These limitations hinder the processability and practical application of QD-based TTA-UC materials. Therefore, developing new surface ligands that enable highly efficient NIR TTA-UC with lower ligand coverage is highly desirable.

We report monosubstituted styryl-BODIPY (BDP-1) as a novel surface ligand. An η'_{UC} (normalized to 100%; corrected for the inner-filter effect of rubrene on the upconverted emission) as high as 16.8 ± 0.6% was achieved with only seven ligands per quantum dot. A comparative analysis was conducted with the previously reported ligand 5-CT at low surface coverage on PbS QDs. Although the upconversion performance of PbS/BDP-1/rubrene is comparable to that of PbS/5-CT/rubrene, BDP-1 exhibits markedly superior stability. Furthermore, employing 9,10-bis(phenylethynyl)anthracene (BPEA) as the annihilator, which possesses a higher T_1 energy than rubrene and emits in the cyan region, PbS/BDP-1/BPEA exhibited upconverted emission with a larger anti-Stokes shift (from 808 nm to 480 nm), and the η'_{UC} is 6.5% ± 0.4%, whereas no upconversion signal was detected for PbS/5-CT/BPEA. These results demonstrate that BDP-1, as a new surface ligand, enables NIR-excited QD-based TTA-UC with an enhanced anti-Stokes shift, higher efficiency, and improved stability—features not attainable with previously reported tetracene-derived ligands.

Results and discussion

Boron-dipyrromethene (BODIPY) derivatives have emerged as promising candidates for ligands on QDs due to their tunable energy levels *via* structural modification and superior photostability.[18,19] However, to date, no reports have described the use of BODIPY-based ligands for achieving QD-based NIR TTA-UC. Guided by the bandgap of 808 nm-absorbing PbS QDs, we designed and synthesized a mono-styryl-BODIPY derivative (BDP-1) as a surface ligand, aiming to enable highly efficient NIR TTA-UC with reduced ligand coverage. The target compound (BDP-1) was obtained through a Knoevenagel condensation between compound 1 and compound 2,[20] yielding the BDP-ester intermediate, followed by LiOH-mediated hydrolysis[21] to remove the protecting group (Fig. 1a and Scheme S1). Detailed molecular structural characterization was conducted for all compounds mentioned. The corresponding data are provided in the SI (Fig. S1–S5). Due to the importance of the distance dependence of triplet exciton transfer from the quantum dot to the surface ligand,[22,23] we also designed and synthesized the short-chain ligand BDP-2 (Fig. 1a). However, BDP-2 exhibited very poor solubility in low-polarity solvents such as toluene and chloroform, which hindered effective ligand exchange with PbS QDs and prevented evaluation of its upconversion performance. We also considered employing longer alkyl chains to link the carboxylic acid group to the BODIPY unit; however, this approach would reduce the wavefunction overlap between the QD and ligand, thereby impairing triplet exciton transfer.[22] Thus, the propyl spacer used in the current design represents a favorable compromise.

The T_1 energy level of the BODIPY core is generally around 1.5 eV, as reported in several studies.[24,25] It has been documented that in heavy-atom-containing BODIPY such as di-iodo BODIPYs, the mono-styryl-substituted BODIPY exhibits a reduced T_1 energy level.[26] Our quantum chemical calculations give a T_1 energy level of 1.37 eV for the mono-styryl-substituted BODIPY (see the SI). This result is consistent with the trend observed in these structurally similar heavy-atom systems,[26] supporting the computational result that mono-styryl-substituted BODIPY lowers the T_1 energy of the BODIPY core. Therefore, based on the T_1 energy level of BDP-1, we synthesized PbS QDs with an absorption wavelength at around 800 nm to serve as the light-harvesting unit for enabling NIR-excited QD-based TTA-UC.

PbS QDs with energy levels matching those of BDP-1 were synthesized following a reported method by optimizing the injection temperature of the sulfur precursor (see the SI).[27] The normalized absorption and emission spectra are shown in Fig. 1b. The first excitonic absorption peak of the PbS QDs is located at 831 nm, corresponding to the lowest-energy $1S_e$–$1S_h$ excitonic transition,[28] and the emission peak of the synthesized PbS QDs appears at 960 nm. Transmission electron microscope (TEM) images (Fig. 1c) and the corresponding size distribution analysis (Fig. 1d) of PbS QDs reveal an average particle size of 2.68 ± 0.19 nm, consistent with the calculated diameter of 2.65 nm derived from the absorption spectrum.[29] The bandgap of the PbS QDs, determined using the Tauc plot method,[30] is 1.38 eV. Notably, the PbS QDs exhibit a photoluminescence quantum yield (PLQY) of 79% and a photoluminescence lifetime of 2.65 μs. The decay profile, well-fitted by a single-exponential function (Fig. S6), indicates that the recombination process is dominated by a single radiative pathway, suggesting high-quality PbS QDs with minimal surface defects. Key photophysical parameters of the PbS QDs are summarized in Table S1. The absorption and fluorescence spectra of BDP-1 are shown in Fig. 1e. BDP-1 exhibits a maximum absorption peak at 571 nm with a molar extinction coefficient of 1.82×10^4 M^{-1} cm^{-1}. Its maximum fluorescence emission peak is located at 583 nm, and the S_1 energy level, calculated from the intersection of the absorption and emission spectra, is 2.15 eV. The absolute fluorescence quantum yield and fluorescence lifetime of BDP-1 are 96% and 3.88 ns (Fig. S7), respectively. The photophysical parameters of BDP-1 are summarized in Table S2.

The carboxylic acid group on BDP-1 facilitates ligand exchange with the native ligands of PbS QDs, enabling the anchoring of BDP-1 onto the PbS QD surfaces. Following a reported method,[15] the $\langle N_{BDP\text{-}1} \rangle$ was determined from the absorption spectra of PbS/BDP-1 (Fig. 2a, b and Table S3). At a BDP-1 concentration of 400 μM for ligand exchange, approximately seven ligands were anchored per PbS QD on average. Compared to the absorption spectrum of free BDP-1 in solution, the absorption peak of BDP-1 on the PbS QD surface exhibited a redshift and broadening, indicating deprotonation of the

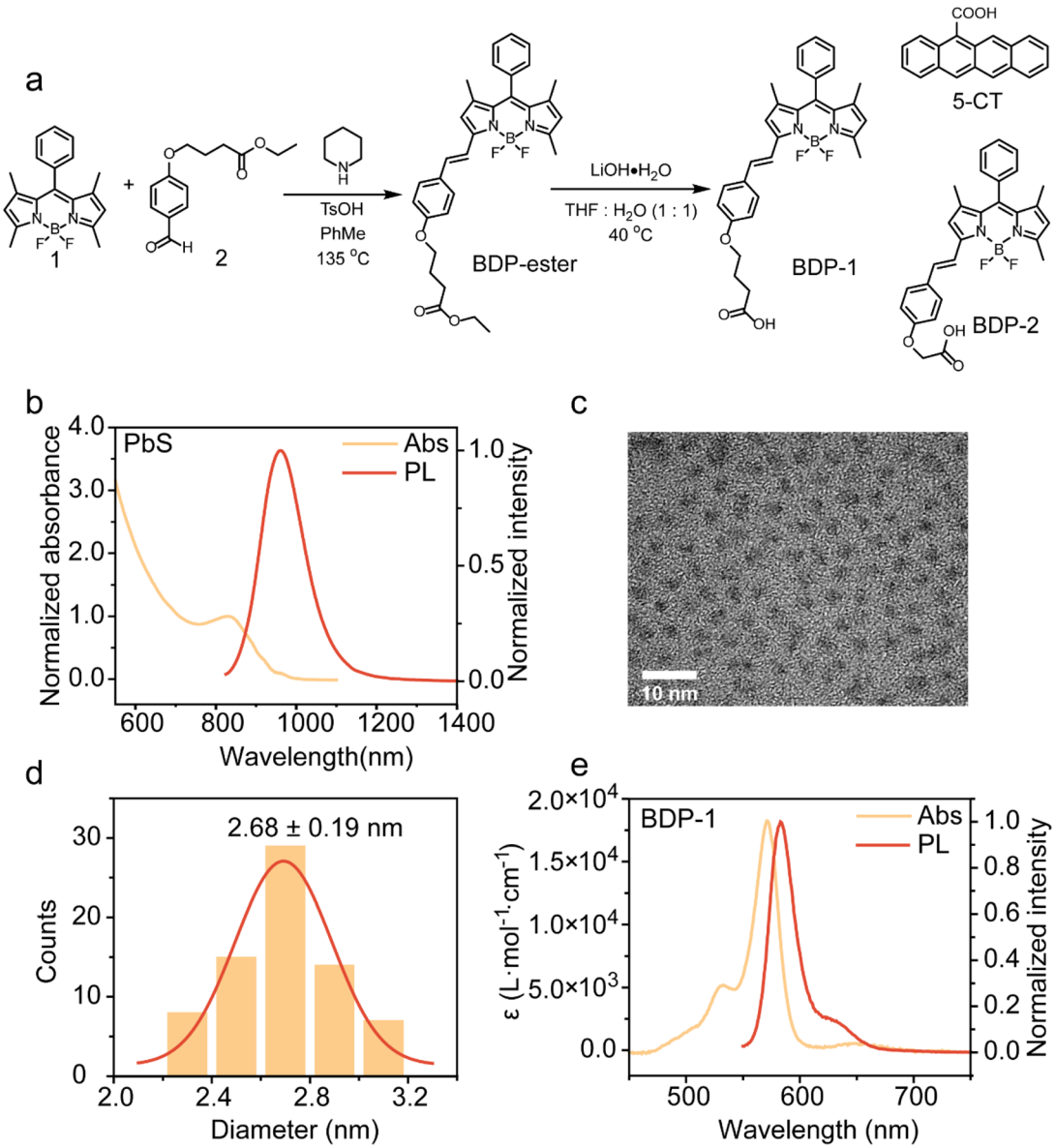

Fig. 1 Preparation process of the surface ligand and properties of PbS QDs and the surface ligand. (a) Preparation process of the BODIPY-based surface ligand (BDP-1) and molecular structures of 5-CT and BDP-2. (b) Normalized absorption spectra (normalized to the first excitonic absorption peak of PbS QDs set to 1) and normalized fluorescence emission spectra of PbS QDs in toluene (1 μM). (c) Transmission electron microscope (TEM) image of PbS QDs. (d) Size distribution histogram with the Gaussian fit of PbS QDs. (e) Absorption and normalized fluorescence emission spectra of BDP-1 in $CHCl_3$ (10 μM).

carboxylic acid group and successful anchoring to the PbS QDs.[31]

We further investigated the chemical behavior of BDP-1 anchored on PbS QD surfaces using 800 MHz ^{1}H NMR spectroscopy. ^{1}H NMR spectra of free BDP-1 and PbS/BDP-1 were collected (Fig. S8). In solution, free BDP-1 exhibits rapid molecular motion, resulting in a highly uniform magnetic environment for all proton atoms, and thus sharp, narrow resonance peaks. For instance, the pyrrole protons labeled 1 and 2 of free BDP-1 appear at 6.54 ppm and 5.98 ppm, respectively. In contrast, when BDP-1 is anchored on the PbS QD surfaces, its molecular motion is significantly restricted, leading to slowed tumbling and rotation.[32–34] This effect causes a substantial reduction in the transverse relaxation time (T_2), directly resulting in broadened and less intense NMR signals.[35] This line-broadening effect is particularly pronounced under a high magnetic field of 800 MHz.[36] The resonance corresponding to the pyrrole proton adjacent to the styryl substituent shifts to 6.58 ppm in PbS/BDP-1, indicating strong electronic coupling between BDP-1 and the PbS QDs. This interaction is expected to facilitate triplet exciton transfer from the PbS QDs to BDP-1.

We subsequently investigated the triplet exciton transfer from PbS QDs to BDP-1. Under 808 nm excitation, the

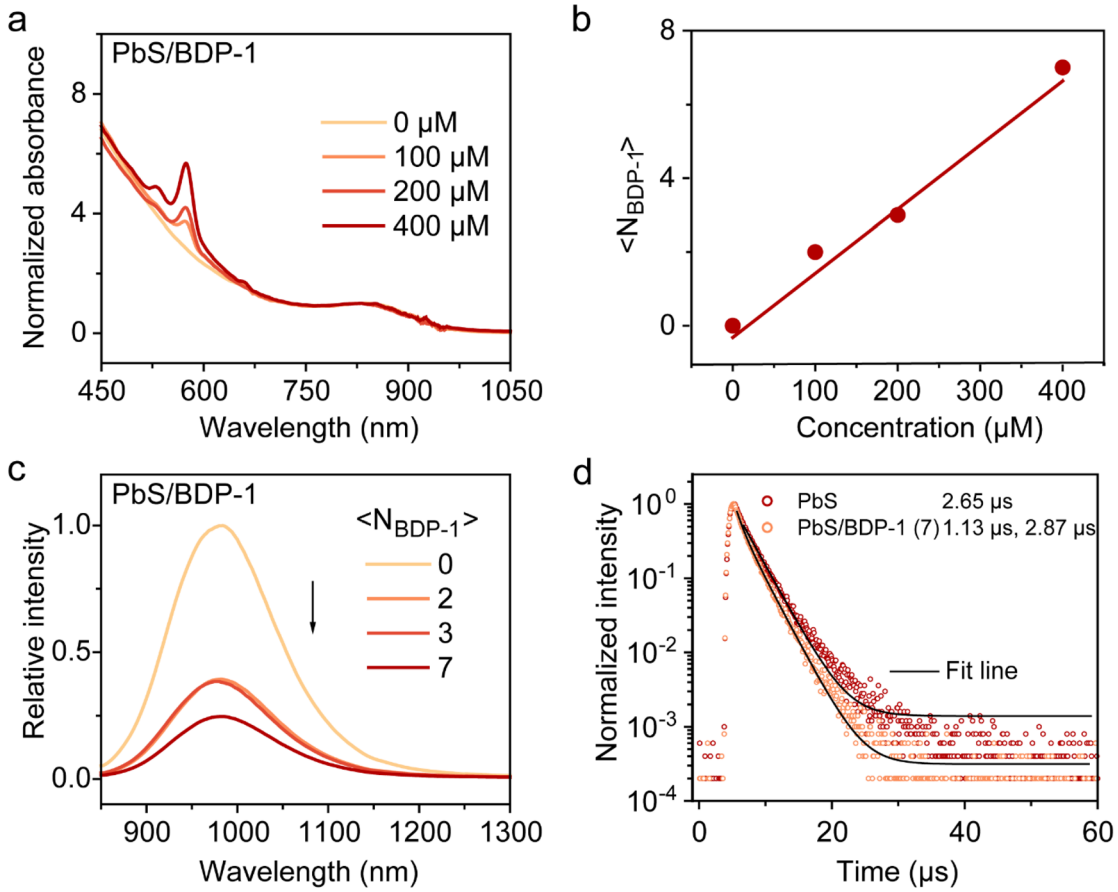

Fig. 2 Photophysical properties of PbS/BDP-1. (a) Normalized absorption spectra of PbS QDs (normalize the first excitonic absorption peak of PbS QDs to 1) after ligand exchange with BDP-1 at different concentrations (0, 100, 200, and 400 μM) in toluene, and the concentration of PbS is 10 μM. (b) The average number of BDP-1 per PbS QD ($<N_{BDP\text{-}1}>$) after ligand exchange with BDP-1 at different concentrations (0, 100, 200, and 400 μM). (c) Relative photoluminescence intensity of PbS with various $<N_{BDP\text{-}1}>$ (0, 2, 3, 7) in argon-saturated toluene. (d) The photoluminescence lifetime of the PbS moiety in PbS/BDP-1, with an average of seven BDP-1 ligands per PbS QD.

photoluminescence intensity of PbS QDs in PbS/BDP-1 was significantly lower than that of pristine PbS QDs (Fig. 2c), suggesting triplet exciton transfer from the *PbS QDs to BDP-1. The photoluminescence lifetime of the PbS moiety in PbS/BDP-1 was measured. With an average of seven BDP-1 ligands per PbS QD, the lifetime of the PbS moiety in PbS/BDP-1 decreased from 2.65 μs to 1.13 μs (Fig. 2d). Due to the close energy alignment between the PbS bandgap and the T_1 level of BDP-1, reverse triplet energy transfer from ^{3}BDP-1* back to the PbS QDs occurs. The shorter-lived component corresponds to forward triplet energy transfer from the *PbS QD to BDP-1, while the longer-lived component arises from this reverse transfer process (Fig. 2d). The triplet–triplet energy transfer efficiency was calculated based on the photoluminescence lifetime of the shorter-lived component. The triplet exciton transfer efficiency was determined to be 57.4%. The triplet energy transfer efficiency calculated from time-resolved fluorescence spectroscopy is slightly lower than that obtained from femtosecond transient absorption measurements (read below). This discrepancy is likely attributed to the presence of reverse triplet energy transfer within PbS/BDP-1.

To rule out the possibility that the observed quenching originated from surface defect formation during ligand exchange, we performed a control experiment using 9-anthracenecarboxylic acid (ACA), and obtained $T_1 = 1.83$ eV,[37] which is higher than the bandgap of PbS QDs. The results indicated that ACA-modified PbS QDs exhibited no significant quenching in either steady-state photoluminescence intensity (Fig. S9a) or fluorescence lifetime (Fig. S9b). This confirms that the ligand exchange process itself does not cause photoluminescence quenching of PbS QDs, thereby verifying that the emission quenching in PbS/BDP-1 stems from efficient triplet exciton transfer from the PbS QDs to BDP-1.

We investigated the potential for photoinduced electron transfer from *PbS QDs to BDP-1 by measuring the photoluminescence intensity and lifetime of the PbS moiety in PbS/BDP-1 dispersed in nonpolar (toluene) and polar (chloroform) solvents. No significant differences were observed in either the photoluminescence intensity (Fig. S10a) or lifetime (Fig. S10b) between the two solvents. These results indicate that excited-state transfer from *PbS to BDP-1 occurs predominantly *via* a triplet energy transfer pathway, generating ^{3}BDP-1*, rather than through a photoinduced electron-transfer mechanism.

To investigate the exciton transfer dynamics between *PbS QDs and their surface ligand (BDP-1), we employed femtosecond transient absorption spectroscopy (fs-TAS) to determine the triplet exciton transfer rate from photoexcited PbS QDs to BDP-1. We first characterized the photophysical transient properties of free BDP-1 and pristine PbS QDs using fs-TA spectra. Under 500 nm pulsed excitation, the fs-TA spectra of BDP-1 were recorded from 2 to 7000 ps (Fig. 3a). Photoexcitation generates the singlet excited state of BDP-1 (^{1}BDP-1*), giving rise to ground-state bleaching (GSB) signals centered at 510 nm and 576 nm. The negative peak at 636 nm is attributed to stimulated emission (SE) from ^{1}BDP-1*. When exciting pristine PbS QDs at 750 nm, an exciton bleach (XB) signal appears in the 740–910 nm region, along with a broad excited-state absorption (ESA) band between 480–700 nm (Fig. 3b). Regarding PbS/BDP-1, fs-TA spectra were collected under 750 nm pulsed light excitation (Fig. 3c), which selectively excites the PbS units without directly exciting BDP-1. The composite also exhibits an XB signal in the 750–910 nm region; however, its recovery is significantly accelerated compared to that of pristine PbS QDs as shown in Fig. 3b. By comparing the XB decay dynamics of PbS and PbS/BDP-1 (Fig. 3d), the exciton transfer rate from PbS QDs to BDP-1 was determined to be $k_{TET} = 1.15 \times 10^{10}$ s^{-1} (where $k_{TET} = 1/\tau_{TET}$). Based on a detailed analysis of fs-TA spectra and following the established protocol,[12] the triplet exciton transfer efficiency from the *PbS QDs to BDP-1 (with seven surface ligands) was determined to be 65.4%. The red shift of the XB in PbS/BDP-1 relative to pristine PbS QDs arises from the size-dependent bandgap of the QDs. The as-synthesized PbS QDs exhibit a size distribution, leading to a corresponding distribution of bandgaps. Smaller QDs have wider bandgaps, resulting in a larger energy-gap driving force relative to the triplet energy level of BDP-1, which facilitates faster triplet exciton transfer. Conversely, larger QDs exhibit slower transfer rates due to the reduced driving force. This size-dependent variation in triplet exciton transfer rates collectively accounts for the overall red shift of XB observed in PbS/BDP-1. Due to the intrinsically weak signal of BDP-1*, which is obscured by the strong ESA from PbS, the formation of BDP-1*-related features could not be directly observed in Fig. 3c. We therefore applied a double-difference method[13] to extract the spectral contribution of BDP-1* in PbS/BDP-1. The resulting double-difference spectra show a GSB signal of BDP-1* that aligns well with its absorption profile (Fig. S11), providing further support for the above conclusions.

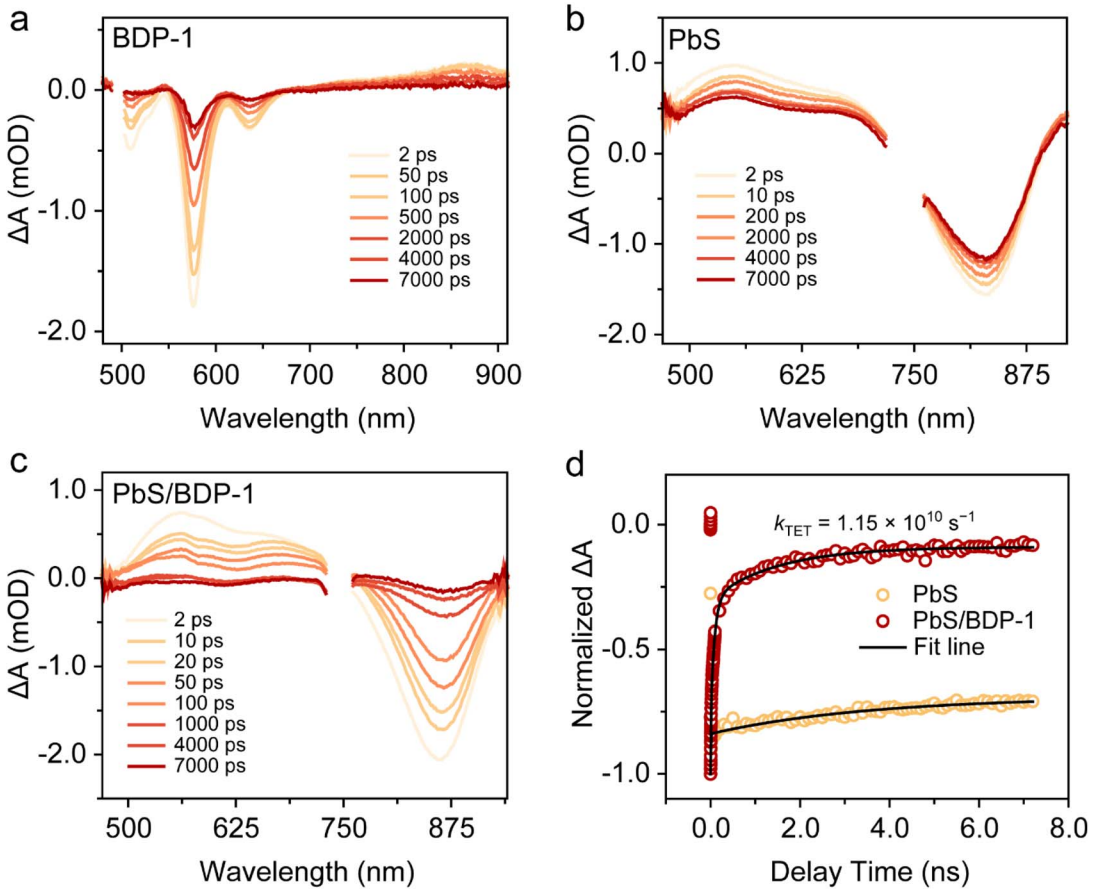

Fig. 3 Ultrafast spectroscopic analysis of exciton transfer between PbS QDs and surface ligand BDP-1. (a) Femtosecond transient absorption (fs-TA) spectra of BDP-1; $\lambda_{ex} = 500$ nm. (b) fs-TA spectra of PbS QDs; $\lambda_{ex} = 750$ nm. (c) fs-TA spectra of PbS/BDP-1; $\lambda_{ex} = 750$ nm. (d) Normalized exciton bleaching (XB) kinetics of PbS and PbS/BDP-1.

Given the high efficiency of triplet exciton transfer observed in PbS QDs with low surface coverage of BDP-1, we investigated the upconversion performance of the hybrid PbS/BDP-1, using rubrene as the annihilator, in argon-saturated toluene. First, the influence of BDP-1 surface coverage on upconversion luminescence was examined. As shown in Fig. 4a, the upconversion intensity gradually increased as the <N_{BDP-1}> per PbS QD increased from 2 to 7. The maximum upconversion intensity (bright yellow emission, inset of Fig. 4a) was achieved at an average of 7 BDP-1 ligands per QD. We investigated the effect of rubrene concentration on upconverted emission. We measured the upconverted emission intensity at various rubrene concentrations. As shown in Fig. S12, the emission intensity increased gradually with higher rubrene concentration; however, beyond 10 mM, no significant further enhancement was observed. Without spectral correction (*i.e.*, without accounting for the inner-filter effect), the integrated upconverted emission areas at rubrene concentrations of 5, 10, and 20 mM were 11.30-, 25.80-, and 25.77-fold, respectively, relative to that at 1 mM (Fig. S12a). Thus, increasing the concentration from 10 to 20 mM did not result in a noticeable increase in emission intensity. High rubrene concentrations introduce a pronounced inner-filter effect. After spectral correction, the integrated emission areas increased to 14.95-, 37.03-, and 43.33-fold at 5, 10, and 20 mM, respectively, compared with that of the 1 mM reference (Fig. S12b). These corrected data indicate that increasing the concentration from 10 to 20 mM still provides some enhancement in upconverted emission. Based on these results, we selected 20 mM rubrene for subsequent TTA-UC measurements.

We further quantified the effect of <N_{BDP-1}> on the η'_{UC}. The highest η'_{UC} of 16.8% ± 0.6% was obtained at 7 BDP-1 ligands per QD. Additionally, the excitation intensity dependence of the upconversion emission was measured to determine the threshold power density (I_{th}) (Fig. 4b). The upconversion intensity increased progressively with excitation intensity, and the corresponding double-logarithmic plot exhibited a characteristic transition from quadratic to linear dependence (Fig. 4c), consistent with typical TTA-UC behavior. The I_{th} was determined to be 24.0 W cm^{-2}. The time-resolved upconversion photoluminescence spectrum revealed a decay lifetime of 56.7 μs for PbS/BDP-1/rubrene (Fig. 4d), further confirming that the observed emission originates from a TTA mechanism.

We attempted to determine whether a higher average number of BDP-1 on the PbS QD surface could further enhance

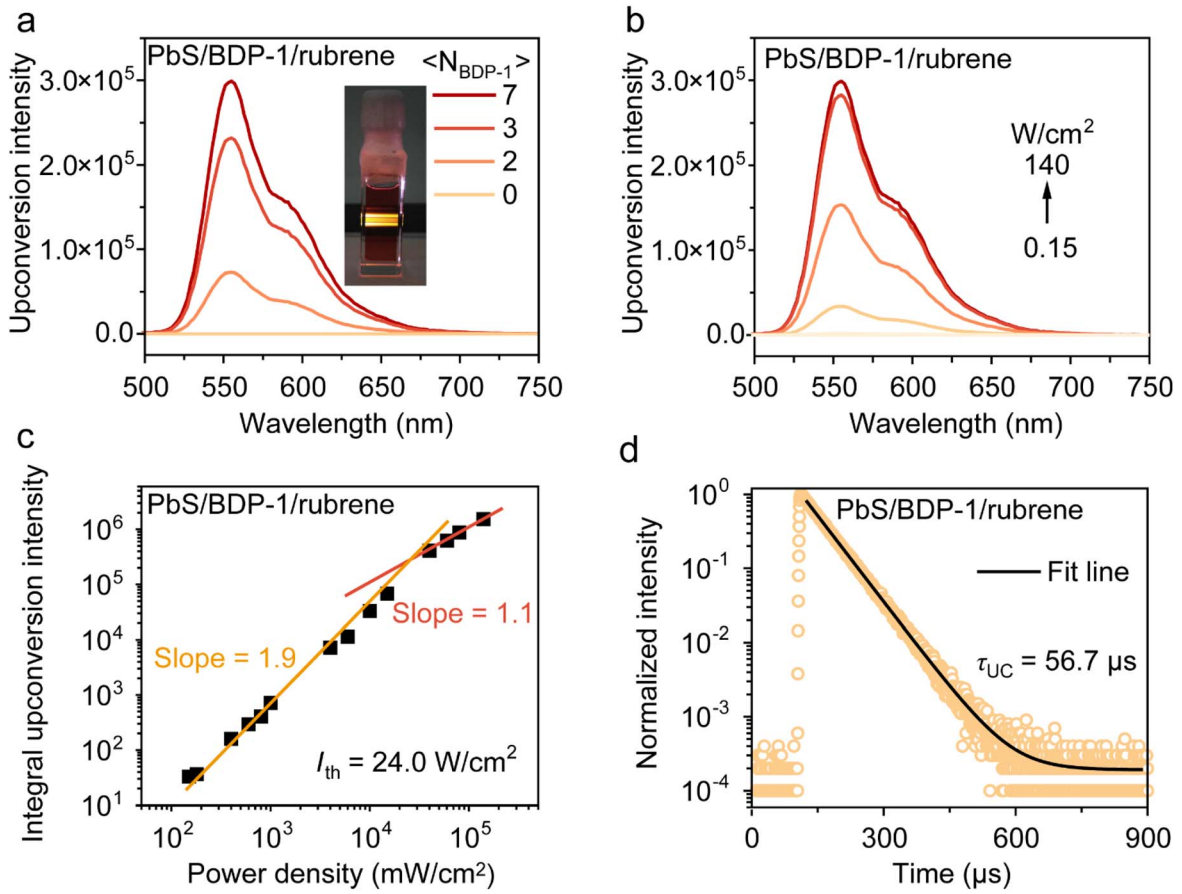

Fig. 4 Photon upconversion performance of PbS/BDP-1/rubrene. (a) Upconversion spectra in the presence of PbS/BDP-1 (sensitizer), rubrene (annihilator), <N_{BDP-1}> (0, 2, 3, 7), λ_{ex} = 808 nm. The inset photograph shows yellow upconversion under 808 nm excitation. (b) Power-dependent upconversion spectra of PbS/BDP-1/rubrene with various power densities (0.15–140 W cm^{-2}) at 808 nm. (c) Dependence of the upconversion intensity of PbS/BDP-1/rubrene on the incident power density at 808 nm; I_{th} = 24.0 W cm^{-2}. (d) Time-resolved upconversion spectrum of PbS/BDP-1/rubrene under pulsed 808 nm excitation.

the upconversion performance. Upon increasing the concentration of BDP-1 to 1600 μM during ligand exchange, the average number of BDP-1 ligands per PbS QD was estimated to be approximately 28, based on its molar extinction coefficient (Fig. S13). We subsequently measured the η'_{UC} of PbS/BDP-1/rubrene (17.6% ± 0.4%). Compared to PbS/BDP-1 with seven surface ligands, the η'_{UC} showed some improvement, although the increase was no longer substantial. This observation suggests that the triplet exciton transfer efficiency from *PbS QDs to BDP-1 approaches saturation at relatively low surface ligand coverage.

To highlight the advantages of BDP-1 as a new surface ligand for NIR-excited QD-based TTA-UC, we evaluated the photon upconversion performance of PbS/BDP-1/rubrene against PbS/5-CT/rubrene, which incorporates the widely recognized ligand 5-CT.[12,15] Since this study focuses on upconversion performance at low surface ligand coverage, TTA-UC samples with an average of two and seven ligands per quantum dot were selected for comparison. The molecular structure of 5-CT is shown in Fig. 1a or S14a. We constructed QD-based photosensitizers (PbS/5-CT), which, in combination with the annihilator rubrene, enable TTA-UC. Owing to the low number of 5-CT molecules attached to the PbS QD surface, no significant effect on the dispersibility of the PbS QDs in solution was observed. When the ligand number was 7, the upconversion performance of PbS/BDP-1/rubrene was comparable to that of PbS/5-CT/rubrene (Fig. S14b and c). We further compared the air stability of the ligands BDP-1 and 5-CT. After 166 hours, the BDP-1 ligand showed no significant degradation, whereas 5-CT was almost completely degraded within 103 hours (Fig. S14d).

Unlike 5-CT, the newly developed ligand BDP-1 has a higher T_1 energy level, allowing it to sensitize annihilators with higher triplet energies, such as 9,10-bis(phenylethynyl)anthracene (BPEA). Compared to rubrene, BPEA demonstrates significantly improved photostability and emits in the cyan region (460–530 nm), resulting in a substantially larger anti-Stokes shift during the upconversion process. Using PbS/BDP-1 as the photosensitizer under 808 nm excitation, we investigated the effect of BPEA concentration on the upconversion emission spectra. The upconverted intensity increased gradually as the BPEA concentration was increased from 2 mM to 10 mM (Fig. 5a). Due to the limited solubility of BPEA in toluene, higher concentrations could not be tested; therefore, 10 mM BPEA was selected for further study. The photograph of the upconverted emission

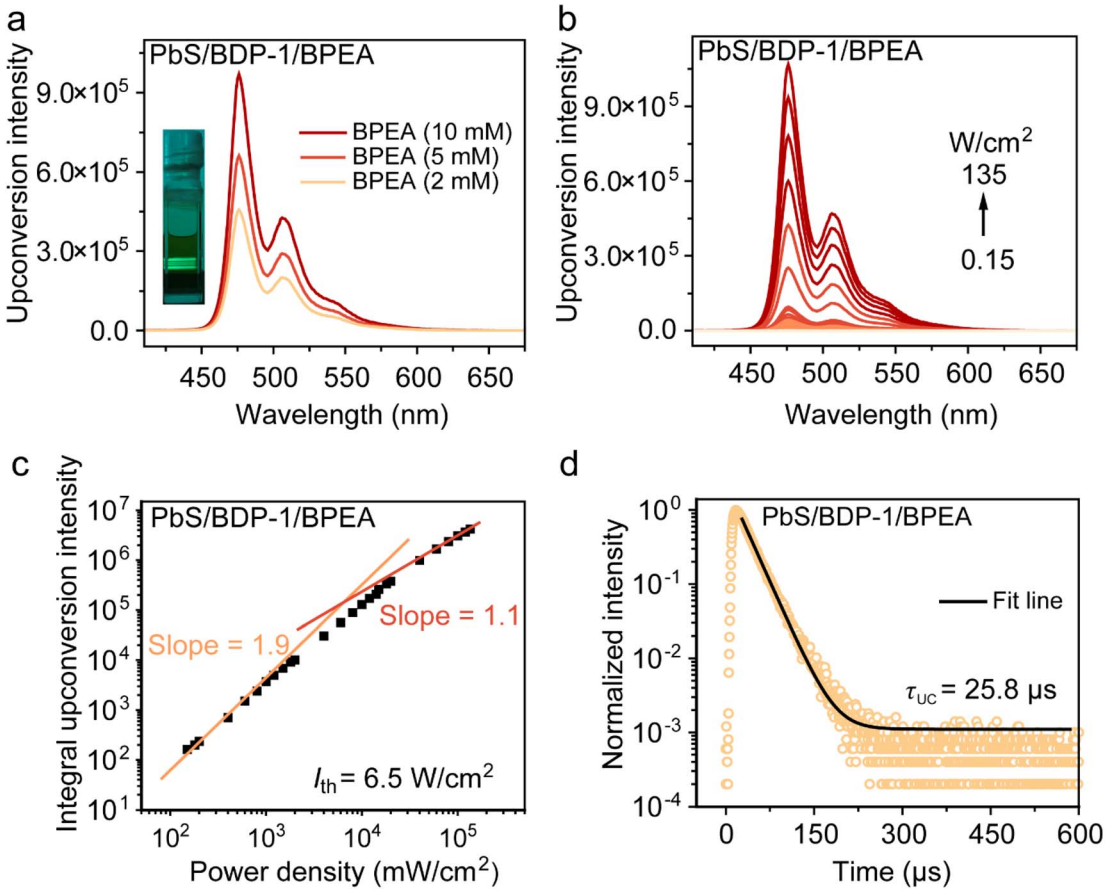

Fig. 5 Photon upconversion performance of PbS/BDP-1/BPEA. (a) Upconversion spectra in the presence of PbS/BDP-1 (sensitizer) and BPEA (annihilator); the BPEA concentration was increased from 2 mM to 10 mM; $\lambda_{ex} = 808$ nm. The inset photograph shows green upconversion under 808 nm excitation. (b) Power-dependent upconversion spectra of PbS/BDP-1/BPEA with various power densities (0.15–135 W cm^{-2}) at 808 nm. (c) Dependence of the upconversion intensity of PbS/BDP-1/BPEA on the incident power density at 808 nm; $I_{th} = 6.5$ W cm^{-2}. (d) Time-resolved upconversion spectrum of PbS/BDP-1/BPEA under pulsed 808 nm excitation.

from PbS/BDP-1/BPEA shows predominantly cyan emission, with an anti-Stokes shift substantially larger than that observed for PbS/BDP-1/rubrene (inset of Fig. 5a). Power-dependent upconversion measurements yielded a threshold power density of 6.5 W cm^{-2} for PbS/BDP-1/BPEA (Fig. 5b and c), and the upconverted emission lifetime was determined to be 25.8 μs, confirming that the cyan emission originates from a TTA process (Fig. 5d). The corrected upconversion efficiency of PbS/BDP-1/BPEA was further determined to be 6.5% ± 0.4%. Under the same experimental conditions, we did not observe any upconverted emission from PbS/5-CT/BPEA. These results demonstrate that BDP-1 not only exhibits enhanced stability but also enables a greater anti-Stokes shift, a performance not achieved with the previously reported 5-CT surface ligand.

Conclusions

This work presents, for the first time, a carboxyl-functionalized mono-styryl BODIPY ligand designed to address the common limitations of polycyclic aromatic ligands, such as difficult derivatization, poor solubility, and limited modification sites. Experimental results demonstrate a high triplet exciton transfer efficiency of 65.4% as determined by femtosecond transient absorption spectroscopy, which can be achieved even with low surface coverage of the ligand. Using rubrene as the annihilator, the PbS/BDP-1/rubrene system exhibits a high upconversion efficiency of 16.8% ± 0.6% with only seven ligands per quantum dot. Compared to conventional tetracene derivatives, this ligand features a higher T_1 energy level, enabling effective synergy with the blue-green emitter BPEA and thereby extending the anti-Stokes shift in near-infrared-excited quantum dot-based triplet–triplet annihilation upconversion. And the corrected upconversion efficiency of the PbS/BDP-1/BPEA system reaches 6.5% ± 0.4%. This result represents a significant advancement in expanding the spectral window of QD-based TTA-UC into the cyan-blue region. These findings suggest that BODIPY chromophores can serve as stable surface ligands on quantum dots, providing a reliable route toward high-performance upconversion luminescence and offering a novel ligand design strategy to advance the practical application of quantum dot-based photon upconversion materials.

Author contributions

R. L. executed the experimental synthesis and characterization, analyzed the data and wrote the manuscript. L.-H. J., M.-Y. Z., and H.-J. F. analyzed the data. L. X. performed femtosecond transient absorption spectroscopy. D.-X. G. carried out theoretical calculations. L.-L. H. contributed to the preparation of the manuscript. L. H. and D.-W. P. conceptualised, coordinated and supervised the project.

Conflicts of interest

There are no conflicts to declare.

Data availability

The data supporting the findings of this study are available within the paper and its supplementary information (SI) files. Raw data are available from the corresponding author upon reasonable request. Supplementary information is available. See DOI: https://doi.org/10.1039/d6sc00714g.

Acknowledgements

This work was supported by the National Natural Science Foundation of China (No. 22293032, 22293030, and 22174076), the Key Research and Development Program of Guangdong Province (No. 2023B0101190004), the "Frontiers Science Center for New Organic Matter", Nankai University (63181206), "the Fundamental Research Funds for the Central Universities", Nankai University (63201024), and the Tianjin Natural Science Foundation (19JCQNJC02400 and 22JCQNJC01600). L. H. is thankful for the financial support provided by the research start-up fund of Nankai University. We thank the Haihe Laboratory of Sustainable Chemical Trans-formations for financial support.

Notes and references

1 T. N. Singh-Rachford and F. N. Castellano, *Coord. Chem. Rev.*, 2010, **254**, 2560–2573.
2 J. Zhao, S. Ji and H. Guo, *RSC Adv.*, 2011, **1**, 937–950.
3 J. Zhao, W. Wu, J. Sun and S. Guo, *Chem. Soc. Rev.*, 2013, **42**, 5323–5351.
4 L. Huang, W. Wu, Y. Li, K. Huang, L. Zeng, W. Lin and G. Han, *J. Am. Chem. Soc.*, 2020, **142**, 18460–18470.
5 W. Liang, C. Nie, J. Du, Y. Han, G. Zhao, F. Yang, G. Liang and K. Wu, *Nat. Protoc.*, 2023, **17**, 346–353.
6 B. D. Ravetz, A. B. Pun, E. M. Churchill, D. N. Congreve, T. Rovis and L. M. Campos, *Nature*, 2019, **565**, 343–346.
7 J. Xu, P. Yang, M. Sun, H. Bi, B. Liu, D. Yang, S. Gai, F. He and J. Lin, *ACS Nano*, 2017, **11**, 4133–4144.
8 Y. Niihori, T. Kosaka and Y. Negishi, *Mater. Horiz.*, 2024, **11**, 2304–2322.
9 R. Sun, J. Zang, R. Lai, W. Yang and B. Ji, *J. Am. Chem. Soc.*, 2024, **146**, 17618–17623.
10 L.-H. Jiang, X. Miao, M.-Y. Zhang, J.-Y. Li, L. Zeng, W. Hu, L. Huang and D.-W. Pang, *J. Am. Chem. Soc.*, 2024, **146**, 10785–10797.
11 K. T. Chang, W. Liang, S. Gong, P. H. Yeung, J. Feng, X. Chen and H. Lu, *J. Am. Chem. Soc.*, 2025, **147**, 14015–14023.
12 Z. Huang, Z. Xu, M. Mahboub, Z. Liang, P. Jaimes, P. Xia, K. R. Graham, M. L. Tang and T. Lian, *J. Am. Chem. Soc.*, 2019, **141**, 9769–9772.
13 Z. Huang and M. L. Tang, *J. Am. Chem. Soc.*, 2017, **139**, 9412–9418.
14 R. Weiss, Z. A. VanOrman, C. M. Sullivan and L. Nienhaus, *ACS Mater. Au*, 2022, **2**, 641–654.
15 M. Mahboub, Z. Huang and M. L. Tang, *Nano Lett.*, 2016, **16**, 7169–7175.

16 Z. Huang, Z. Xu, M. Mahboub, X. Li, J. W. Taylor, W. H. Harman, T. Lian and M. L. Tang, *Angew. Chem., Int. Ed.*, 2017, **56**, 16583–16587.
17 A. Maliakal, K. Raghavachari, H. Katz, E. Chandross and T. Siegrist, *Chem. Mater.*, 2004, **16**, 4980–4986.
18 A. Loudet and K. Burgess, *Chem. Rev.*, 2007, **107**, 4891–4932.
19 C. S. Mahanta, V. Ravichandiran and S. P. Swain, *ACS Appl. Bio Mater.*, 2023, **6**, 2995–3018.
20 L. Huang, X. Yu, W. Wu and J. Zhao, *Org. Lett.*, 2012, **14**, 2594–2597.
21 T. Piou, L. Neuville and J. Zhu, *Org. Lett.*, 2012, **14**, 3760–3763.
22 X. Li, Z. Huang, R. Zavala and M. L. Tang, *J. Phys. Chem. Lett.*, 2016, **7**, 1955–1959.
23 Z. Xu, Z. Huang, C. Li, T. Huang, F. A. Evangelista, M. L. Tang and T. Lian, *ACS Appl. Mater. Interfaces*, 2020, **12**, 36558–36567.
24 L. Huang and J. Zhao, *J. Mater. Chem. C*, 2015, **3**, 538–550.
25 W. Lv, Y. Li, F. Li, X. Lan, Y. Zhang, L. Du, Q. Zhao, D. L. Phillips and W. Wang, *J. Am. Chem. Soc.*, 2019, **141**, 17482–17486.
26 W. Wu, H. Guo, W. Wu, S. Ji and J. Zhao, *J. Org. Chem.*, 2011, **76**, 7056–7064.
27 M. Mahboub, H. Maghsoudiganjeh, A. M. Pham, Z. Huang and M. L. Tang, *Adv. Funct. Mater.*, 2016, **26**, 6091–6097.
28 M. S. Gaponenko, N. A. Tolstik, A. A. Lutich, A. A. Onushchenko and K. V. Yumashev, *Phys. E*, 2013, **53**, 63–65.
29 I. Moreels, K. Lambert, D. Smeets, D. De Muynck, T. Nollet, J. C. Martins, F. Vanhaecke, A. Vantomme, C. Delerue, G. Allan and Z. Hens, *ACS Nano*, 2009, **3**, 3023–3030.
30 S. Kumar, S. Kumar, P. Sharma, V. Sharma and S. C. Katyal, *J. Appl. Phys.*, 2012, **112**, 123512.
31 Y. Deree, A. Levi, X. Li, O. Gidron and U. Banin, *Nanoscale Horiz.*, 2025, **10**, 1997–2002.
32 Z. Hens and J. C. Martins, *Chem. Mater.*, 2013, **25**, 1211–1221.
33 B. Zeng, G. Palui, C. Zhang, N. Zhan, W. Wang, X. Ji, B. Chen and H. Mattoussi, *Chem. Mater.*, 2018, **30**, 225–238.
34 J. H. Kim, H. Park, T.-G. Kim, H. Lee, S. Jun, E. Lee, W. S. Jeon, J. Chung and I.-S. Jung, *Sci. Rep.*, 2021, **11**, 19889.
35 V. V. S. Uppala, C. Y. Dones Lassalle, J. E. Kelm, A. M. Camp, M. A. ter Horst, A. R. Esker, J. L. Dempsey and L. A. Madsen, *ACS Nano*, 2025, **19**, 27246–27258.
36 J. De Roo, N. Yazdani, E. Drijvers, A. Lauria, J. Maes, J. S. Owen, I. Van Driessche, M. Niederberger, V. Wood and J. C. Martins, *Chem. Mater.*, 2018, **30**, 5485–5492.
37 Z. Huang, X. Li, M. Mahboub, K. M. Hanson, V. M. Nichols, H. Le, M. L. Tang and C. J. Bardeen, *Nano Lett.*, 2015, **15**, 5552–5557.